Published in final edited form as:

Alcohol Clin Exp Res. 2018 September ; 42(9): 1769–1782. doi:10.1111/acer.13820.

Combined Face-Brain Morphology and Associated Neurocognitive Correlates In Fetal Alcohol Spectrum Disorders

Michael Suttie, Ph.D.[1,2], **Jeffrey R. Wozniak, Ph.D.**[3], **Scott E. Parnell, Ph.D.**[4], **Leah Wetherill, M.Sc.**[5], **Sarah N. Mattson, Ph.D.**[6], **Elizabeth R. Sowell, Ph.D.**[7], **Eric Kan, B.Sc.**[7], **Edward P. Riley, Ph.D.**[6], **Kenneth L. Jones, M.D.**[8], **Claire Coles, Ph.D.**[9], **Tatiana Foroud, Ph.D.**[5], **Peter Hammond, Ph.D.**[1,2], and **CIFASD**[1,2]

[1]Nuffield Department of Women's and Reproductive Health, University of Oxford, UK;

[2]Big Data Institute, University of Oxford, UK;

[3]Department of Psychiatry, University of Minnesota, Minneapolis, USA;

[4]Department of Cell Biology and Physiology, University of North Carolina, Chapel Hill, USA;

[5]Department of Medical and Molecular Genetics, Indiana University School of Medicine, Indianapolis, USA;

[6]Department of Psychology, San Diego State University, San Diego, California, USA;

[7]Department of Pediatrics, University of Southern California and Children's Hospital Los Angeles, USA;

[8]Department of Pediatrics, School of Medicine, UCSD, San Diego, USA;

[9]Department of Psychiatry and Behavioral Sciences, Emory University School of Medicine, Atlanta, USA;

Abstract

Background: Since the 1970s, a range of facial, neurostructural and neurocognitive adverse effects have been shown to be associated with prenatal alcohol exposure. Typically, these effects are studied individually and not in combination. Our objective is to improve the understanding of the teratogenic effects of prenatal alcohol exposure by simultaneously considering face-brain morphology and neurocognitive measures.

Methods: Participants were categorized as control (n=47), fetal alcohol syndrome (FAS, n=22) or heavily exposed prenatally, but not eligible for a FAS diagnosis (HE, n=50). Structural brain MRI images and high-resolution 3D facial images were analyzed using dense surface models of features of the face and surface shape of the corpus callosum and caudate nucleus. Asymmetry of the caudate nucleus was evaluated for correlations with neurocognitive measures.

i. Facial growth delineations for FAS, HE and controls are replicated for the caudate nucleus and the corpus callosum.

Correspondence: Professor Peter Hammond, Big Data Institute & Nuffield Department of Obstetrics and Gynaecology, University of Oxford, Oxford, OX3 7FZ, UK, **Tel:** +44 (0) 1865 221004, **Fax**: +44 (0) 1865 769141, peter.hammond@obs-gyn.ox.ac.uk.

ii. Concordance of clinical diagnosis and face based control-FAS discrimination improves when the latter is combined with specific brain regions. In particular, midline facial regions discriminate better when combined with midsagittal profile of the corpus callosum.

iii. A subset of HE individuals was identified with FAS-like caudate nucleus dysmorphism. The average of this HE subset was FAS-like in its facial dysmorphism.

iv. Right-left asymmetry found in the caudate nuclei of controls is not apparent for FAS, is diminished for HE and correlates with neurocognitive measures in the combined FAS and HE population.

Conclusions: Combined morphology analysis of the caudate nucleus, and the corpus callosum, with the face, better identify those with FAS. Caudate nucleus asymmetry was reduced for FAS compared to controls and is strongly associated with general cognitive ability, verbal learning and recall in those with prenatal alcohol exposure. This study further extends the brain-behavior relationships known to be vulnerable to alcohol teratogenesis.

Keywords

3D Facial Analysis; Facial Dysmorphism; Fetal Alcohol Spectrum Disorders; Corpus Callosum; Caudate Nucleus

INTRODUCTION

Fetal alcohol spectrum disorders (FASD) is an umbrella term that encompasses the range of deficits that arise from the teratogenic effects of *in utero* alcohol exposure. At the more severe end of the spectrum is fetal alcohol syndrome (FAS) characterised by distinctive facial dysmorphology, neurocognitive deficits and growth delay (Hoyme et al., 2016). The diagnosis of FAS strongly relies on the identification of specific facial features during a thorough dysmorphology exam undertaken by specialist clinicians. Facial features can often identify individuals at the severe end of the FASD spectrum, but a significant proportion of alcohol-exposed individuals do not present a clear set of phenotypic traits (Jones et al., 2010). Heavily-exposed (HE) individuals with significant in utero exposure to alcohol but without clear facial dysmorphia often go undiagnosed and so fail to receive appropriate support that can be offered to both child and parent. Depending on which guidelines are used for clinical diagnosis, classification without facial features will rely on other criteria regarding confirmed alcohol exposure, central nervous system (CNS) abnormalities and/or a pattern of neurocognitive impairments (Chudley et al., 2005; Hoyme et al., 2016). The HE subgroup accounts for the vast majority of affected individuals. Some estimates suggest the incidence rate is an order of magnitude greater than that for FAS (May et al., 2000).

Previous studies using Dense Surface Model (DSM) based shape analysis have delineated atypical facial morphology for a variety of conditions (Chinthapalli et al., 2012; Cox-Brinkman et al., 2007; Hammond et al., 2005; Heulens et al., 2013). DSM models have an advantage over traditional landmark-based analysis in their potential to assess variation across the entire face surface, utilising 3D shape rather than linear and angular measures or even co-location of landmarks. In previous alcohol-related studies (Suttie et al., 2017, 2013),

we focused on facial dysmorphism across the FASD spectrum with the aim of improving the clinical recognition of associated facial features. In particular, using DSM analysis of facial form, we successfully discriminated between FAS and control individuals, and induced partitions of HE subsets into subgroups with FAS-like and control-like facial dysmorphism and corresponding neurocognitive performance.

Facial and brain dysmorphia associated with FASD have been well characterised independently in the literature. Only a handful of studies to date have investigated correlations between them (Roussotte, 2012; Yang et al., 2012a, 2012b). Notably, previous work utilising DSMs (Lipinski et al., 2012) introduced a simultaneous analysis of face and brain in a murine model of in utero ethanol-exposure at two time points (gestational days 7 and 8.5) and concluded that stage-specific ethanol exposure caused a unique pattern of face-brain dysmorphism. While human studies can never provide alcohol exposure data with such precision, it remains important to understand face-brain correlations in alcohol-exposed populations. In this study, we introduce and apply combined DSM techniques for face-brain shape analysis.

The deleterious and disproportionate effect prenatal alcohol exposure is thought to have on corpus callosum development (McGee, 2005) justifies its selection as a component to evaluate when undertaking combined face-brain analyses. The corpus callosum is the largest myelinated midline structure in the brain primarily responsible for interhemispheric communication. A range of morphological defects have been identified amongst individuals with PAE: reduced callosal volume (Archibald et al., 2001; Sowell et al., 2001); corpus callosum displacement (Sowell et al., 2001); reductions in regional callosal thickness (Yang et al., 2012b); and, shape anomalies at the splenium (Bookstein et al., 2007). Additionally, the incidence of partial or full agenesis of the corpus callosum in PAE individuals is thought to be of the order of 6.8% (Riley et al., 1995). The resulting disruption in development has been associated with a range of neurocognitive and neurobehavioral deficiencies in learning, verbal memory, executive function, social cognition and attention (Mattson et al., 2011).

The diagnostic categories used in this analysis refer to unexposed or minimally exposed controls and two alcohol-exposed groups: fetal alcohol syndrome (FAS), and non-syndromal heavily exposed (HE). FAS individuals were diagnosed using criteria outlined in Table 1, requiring confirmation of facial dysmorphism and neurocognitive deficit as well as growth and brain defects. The HE classification is used where prenatal alcohol exposure (PAE) is confirmed, but clinical requirements for a FAS diagnosis are not met. Individuals in the HE subset remain clinically challenging due to the absence of identifiable characteristic criteria, so they may not receive a diagnosis that acknowledges the contributions of PAE to their neurodevelopmental impairments.

STUDY POPULATION

The Collaborative Initiative on Fetal Alcohol Spectrum Disorders (CIFASD) consortium has recruited several thousand participants who completed clinical examinations, neurobehavioral profiles, 3D face images and MRI scans. For this study, 119 participants were available, the majority from a recently described Caucasian cohort (Suttie et al., 2017),

and some additional subjects of Latin American descent. For each participant in this analysis, we require clinical data, a 3D facial image and an MRI image acquired at a time point close to that of the face. The interval between MRI and 3D face data acquisition is on average three months (SD 4.5 months) with those of greater than nine months excluded from the study. CIFASD recruited participants from four sites across the USA: San Diego (SD), Los Angeles (LA), Atlanta (ATL) and Minneapolis (MN). Self-reported ethnicity data collected for all participants revealed 28 to be of Latin American descent and the remaining of European ancestry. Diagnostic categorization partitioned the dataset into the following classifications: control (n=47); FAS (n=22); HE (n=50). We also use the term 'exposed' for the aggregation of HE and FAS.

CLINICAL ASSESSMENT

Subjects with a history of brain injury, genetic disorders and non-alcohol related neurocognitive deficits were excluded from the study. Each child was examined for growth deficits and FAS facial features independently by a single expert dysmorphologist (KLJ), applying the Hoyme criteria for FASD diagnoses (Hoyme et al. 2016). Philtrum smoothness and upper lip vermillion thickness were scored using the Astley lip-philtrum chart (Astley and Clarren, 2001), and palpebral fissure length (PFL) was measured in millimetres manually by the assessing clinician using a ruler. Maternal alcohol consumption data for timing and dose were not always available. However, confirmation of excessive alcohol consumption comparable to alcohol abuse patterns were recorded for all subjects within the 'exposed' groups. The control group also includes 3 individuals with reported 'minimal' alcohol exposure, where maternal alcohol intake is negligible (< 1 standard drink (US) per week on average and never >2 on any occasion) and does not represent a significant risk to neurodevelopment.

Standardised batteries of neuropsychological tests were also undertaken, with 70 subjects evaluated using the Differential Ability Scales, Second Edition (DAS-2; Elliott 2007) and the California Verbal Learning Tests for Children (CVLT-C; Delis et al. 1994) as part of a larger battery. The DAS-2 consists of a series of cognitive subtests measuring verbal, nonverbal, and spatial reasoning abilities. The DAS-2 yields a measure of general cognitive ability (GCA) with qualities similar to an intelligence quotient (IQ) score. The CVLT-C is a comprehensive measure of verbal learning and memory.

MATERIALS AND METHODS

Imaging Protocols

3D facial images were captured using a commercial 3D camera (www.3dMd.com) producing 180-degree ear-to-ear images and more than 25,000 mesh points at sub-millimetre accuracy (geometric resolution <0.2mm). Each participant had their 3D photo taken as part of the clinical assessment. Using in-house software (Facemark), the first author manually annotated each face surface with a sparse set of 24 reliable anatomical landmarks (Gwilliam et al., 2006) (Supplementary Fig. S1). High-resolution T1-weighted MRI images were captured across all 4 sites using 3T scanners. In MN and ATL, volumes were collected from a 3T Siemens TIM Trio whole-body magnet, with repetition time (TR) = 2170 ms, echo time

(TE) = 4.330 ms, flip angle = 7°, matrix size = 256 × 256, field of view (FOV) = 256 mm, and voxel size = 1 mm. In LA, images were acquired from a 3T Phillips Achieva magnet with TR = 6.767 ms, TE = 3.196 ms, flip angle = 8°, matrix size = 256 × 256, FOV = 256, and voxel size = 1.2 mm. In SD, images were acquired from a 3T GE Discovery MR750 magnet with TR = 7.648 ms, TE = 3.040 ms, flip angle = 8°, matrix size = 256 × 256, FOV = 256, and voxel size = 1.0 mm.

Corpus Callosum Extraction

Each brain MRI was registered to MNI152 space via FSL's FLIRT (Jenkinson et al., 2012). From a midline slice, a segment was generated from the posterior aspect of the genu to the inferior-most point of the splenium, for both superior and inferior parts of the corpus callosum (Fig S2A). The segments were concatenated to form a continuous midline contour of the corpus callosum (Fig S2B). Equidistant +/− Z points were generated at a fixed distance either side of each vertex and the original contour points were combined to create a thin, artificially triangulated, ribbon-like mesh (Fig S2C), with surface normals computed from the vector product of created edges. An unweighted, sliding-average smoothing algorithm was applied to eliminate noise from the mesh. Three manually placed landmarks (lower point of the splenium, tip of the genu, and the midpoint of the superior arch) were used to generate a clipping plane through the midline of the 3D surface. Surface geometry was extracted from the intersecting points within this plane to produce an accurate representation of a midline contour. The contour was used to produce 30 additional equidistant semi-landmarks between the three original points, calculated using equal geodesic separation on the shortest path along the contour. The resulting semi-landmarks comprise 10 from genu to mid-superior point, 10 from the mid-superior point to the splenium and 10 on the inferior arch from genu to splenium (Fig S2D).

Caudate Nucleus Extraction

Raw MRI images were segmented using an automated multi-atlas pipeline developed by researchers from the Translational Imaging Group at University College London. 20 control MRI atlas images containing 67 manually delineated regions were obtained from the Biomedical Image Analysis Group at Imperial College London (www.brain-development.org). Employing an open source image processing tool, NiftyReg (Modat et al., 2010; Ourselin et al., 2000), we applied an initial image affine registration and non-rigid registration prior to segmentation. Using the multi-STEPS (Multi-label Similarity and Truth Estimation) algorithm in NiftySeg (Cardoso et al. 2013), a multi-atlas based propagation process calculated accurate parcellations for each subject. Thresholding the image as per the original atlas images segmented the caudate nucleus. The selected region contains the extracted body of the nuclei, omitting the inter-connected tail and putamen regions. MicroView (http://microview.parallax-innovations.com), a freely available 3D image viewer and analysis platform, was used to compute the left and right 3D surfaces of the caudate nucleus which were annotated with 6 landmarks using in-house software.

Dense Surface Modelling

DSMs of individual face and brain components were built using in-house software (Hammond and Suttie, 2012). DSM applies a principal component analysis (PCA) to

represent the co-variation of thousands of densely corresponded points, after surface alignment and thin-plate spline warping (Bookstein, 1997) using the sparse set of manually placed anatomical landmarks (Figs. S1, S2C and S3). Single DSM models resynthesize individual 3D surfaces as a weighted linear sum of principal components (PCs) that account for 99% of the shape variation. The standard Euclidean-based metric determines distance and overall shape difference between vectors of weights synthesising individual faces and average faces of homogeneous groups. To analyse morphological covariance between face and brain structures, we apply a technique based on Active Appearance Models (AAM) (Cootes et al. 1998) which originally provided a method to apply PCA to pixel intensity information while taking into account shape variation. Following Cootes et al. (1998), independent vectors of PC values from separate DSM models covering 100% of shape variance are concatenated before undergoing further PCA analysis of the combined representation. A commensuration factor is applied to the model to account for the difference in variance of both models. The resulting combined dense surface models (CDSM) of the separate anatomical components produces PC values expressing shape variance for both structures.

For separate face and brain DSMs, and for combined face-brain, we applied multi-folded classification techniques; closest mean (CM), linear discriminant analysis (LDA) and support vector machines (SVM) in a supervised learning fashion to classify individuals and groups previously categorised clinically. For example, for closest mean classification, we calculated the relative similarity of a face, brain or face-brain surface to the average control or mean FAS subgroup face to discriminate between sets of unseen randomly sampled test examples across 20 cross-validation trials. We determined discrimination between two diagnostic subgroups in terms of the mean area under the receiver operating curves (ROC) of the 20 trials, representing the probability of correctly classifying a pair of randomly selected faces (or brains or face-brain pairs) with each of the pair from a different diagnostic subgroup. Additionally, we estimated the equal error rate (EER) for each ROC to determine classification performance relative to the true positive rate. EER is defined as the point on the ROC where true positive and false positive rates are equal, which we summarize as an average across each of the 20 splits for each classification algorithm.

Individual face and brain signatures are calculated as displacement normalized with respect to displacements at corresponding points on age-matched reference surfaces. In this study, we use 35 consecutively aged controls as references surfaces, and for the construction of age-matched means for individual and FASD group comparisons. Running means generated in this dataset do not cover the age range of the entire alcohol-exposed population. Consequently, those >6 months from their closest generated reference mean are excluded. To portray directional surface displacement, we produce signatures as heat maps representing normalized shape for lateral, vertical, and depth axes. For pairs of signatures, we compute a signature distance by calculating the difference in dysmorphism as the square root of summed squared differences across all surface points. Each signature in the dataset is linked to its closest signature by distance creating signature clusters themselves linked by closest signatures forming a connected signature graph (Hammond and Suttie, 2012) drawn using GraphViz.4.2 (Ellson et al., 2002).

Asymmetry Analysis of the Caudate Nucleus

Asymmetry of a biological component is typically analysed by comparing original and reflected forms (Klingenberg et al. 2002; Hennessy et al. 2005). Similar to previous DSM asymmetry analyses (Hammond et al., 2008; Postema et al., 2017; Schoot et al., 2017), we generated a reflected form of each caudate surface and swapped the left-right landmarks before resampling the surface, effectively generating a dense correspondence of surface points on both left and right sides of the caudate. To consider asymmetry, we constructed a DSM of the combined set of original caudate surfaces and their reflected forms and computed as a simple measure of asymmetry (asymmetry index) as the generalised Euclidean distance between the DSM-based vectors representing each caudate and its reflected form.

The relation of caudate asymmetry indices with DAS-2 and CVLT-C neurocognitive test outcomes were examined for each individual. To determine statistical significance, we computed 2-tailed Pearson correlation coefficients for correlations between the caudate asymmetry indices, and each of the age-adjusted variables of the CVLT-C and DAS-2 tests.

RESULTS

Cohort Characteristics

The male-female split for the 119 subjects was balanced without age distribution differences for FAS and control groups. However, the HE group has a significant majority of male subjects (72%). As expected, we observed the presence of diagnostic severity dependent effects: for head circumference, FAS < HE & control; for height and weight, FAS < HE & control; and for volumetric brain measures (left and right caudate volume and total intracranial volume) FAS & HE < control. Sample characteristics are detailed in Table 2.

Face-Brain Growth and Prenatal Alcohol Exposure

For the controls in this study PC1 for DSMs based on the face (and facial regions) correlates with age ($r^2 = 0.35; p < 0.0001$) and hence reflects growth, with FAS significantly smaller ($p<0.00005$) and HEs marginally smaller than controls (Fig 3). Similarly, these group differences are observed for each of the brain models. In the corpus callosum only DSM, PC1 is representative of growth but does not correlate with age or follow the typical trajectory seen in the face (Fig 1). However, corpus callosum PC1 values show significantly reduced growth for FAS ($p<.00001$) and HE ($p<0.03$) compared to controls. PC1 for the caudate nucleus only DSM has a strong correlation with caudate volume ($r^2 = 0.75$) for controls and exposed groups and shows significantly reduced growth for FAS ($p<0.00001$) and HE ($p<0.002$) compared to controls (Fig 2).

Control-FAS Discrimination based on Face or Brain Morphology alone

We determined agreement of control-FAS clinical categorisation with multi-folded discrimination based on surface shape alone using the full face and smaller localised regions. Each of the 20 folds employed a randomly sampled 90%-training set and a 10%-unseen test set. The same approach was used for the corpus callosum and caudate nucleus, and left-right

segments of the latter. Three supervised learning algorithms (CM, SVM and LDA) produced discrimination results that were highly concordant with clinical diagnosis (Table 3) for both midline facial regions (profile, philtrum, nose and upper-lip vermilions) and non-midline regions (face, eyes, mandible and malar). Generally, the corpus callosum and caudate nucleus (both whole and left and right segments) discriminated as accurately as the facial regions. Equal error rates for each of these tests are shown in the supplementary material (Table S3).

Control-FAS Discrimination based on Combined Face-Brain Morphology

Concordance of clinical diagnosis with control-FAS shape-based discrimination for combined face-brain models was determined as for face and brain separately (Table 4). When combining face and corpus callosum, we observed equal or marginally improved results compared to face and corpus callosum separately. To simplify the results table, and to show where improvements in accuracy occur, Figs. 4 and 5 plot combined face-brain vs face only discrimination results for each facial region. Notably, face-brain combinations show the greatest increase over face-only discrimination rates when combining corpus callosum with midline facial structures; nose, lip vermillion, profile and philtrum (Fig 4A). Combining caudate nucleus with the face increased classification accuracy for the eyes and whole face (Fig 4B) compared to face only. However, improved discrimination rates occurred when combining left caudate nucleus with facial regions (Fig 5). Equal error rates for each of these tests are shown in the supplementary material (Table S4).

Signature graphs of Caudate Nucleus and face partition the heavily exposed (HE) subgroup into FAS-like and control-like subsets

In previous studies (Suttie et al. 2013; Suttie et al. 2017), face based signature graphs containing individuals with PAE partitioned HE subgroups into FAS-like and control-like subsets which correlated with cognitive impairment. We repeated the same approach here to produce signature graphs of exposed individuals using single surface models for both brain components and the full face. Reassuringly, the face signature graph produced a partition of the HE group into FAS-like and control-like subsets (Fig S4) that recapitulated previous results with 22 subjects with an affinity to the FAS cluster and 21 others. The signature graph for the (entire) caudate nucleus (Fig 6) partitioned the HE subgroup into 17 subjects with an affinity to the FAS cluster and 25 others. There was a 66% overlap (12/17) of FAS-like HE partition from the face only graph (Fig S4) with the caudate nucleus graph. As this dataset contains small numbers of controls for each site group, we are unable to generate age-site matched means to control for the different scanner systems used for acquisition. Instead, we construct the same graph labelling each node by site rather than diagnosis to determine if site difference are influencing node connectivity. Using a collapsed form of site-labelled graph (Fig S5), we can calculate an entropy-like measure, dispersion index, to summarise clustering association or dispersion of members of each site (Hammond et al. 2012). Site dispersion coefficients (00B5 ± CI 95%) for the caudate nucleus of the exposed subset for each site are SD=0.77±0.03, MN=0.80±0.04, LA=0.79±0.06, ATL=0.96±0.07 suggesting there is no site based affinity influencing the caudate signature graph.

For the FAS-like subcluster of HE individuals induced in the caudate nucleus signature graph, we generated mean facial signatures for all three axial displacement comparisons (Fig 7B). These show notable similarity to corresponding FAS mean face signatures (Fig 7A) demonstrating FAS-like dysmorphism for both face and caudate shape. We also classified this induced mean face against the control and FAS subsets showing it to be closer to the FAS mean than the control mean for each facial region other than the periorbit (Fig S5).

Application of the same signature graph-based analysis to the corpus callosum failed to induce any clustering of HE individuals amongst FAS nodes. Instead, both HE and FAS nodes were dispersed evenly across the graph indicating a lack of homogeneity in both groups.

Caudate Nucleus Left-Right Asymmetry

In the control-FAS classification results stated above and shown in table 4, we demonstrated improved discrimination rates combining the left caudate with facial regions, compared to combinations with the right caudate. This suggests that asymmetry of the caudate nucleus may play a role in control-FAS discrimination.

We observed a significantly reduced left-right caudate nucleus asymmetry (Fig 8A; $p<0.002$) in the FAS group ($\mu=10.5 \pm 1.59$ SD) compared to the controls ($\mu=12.1 \pm 1.9$ SD). In contrast, the HE group ($\mu=11.5 \pm 1.9$ SD) shows degrees of asymmetry which on average are closer to that of controls (Fig 8B). Within the FAS and control subsets asymmetry indices between sites showed no significant differences (Table S1).

Localised regions of left-right asymmetry can be visualised by heat mapping displacement differences between the mean reflected surfaces for each group against the originals (Fig 9). From the mean original-reflected differences we observe localised directional asymmetries along the anteroposterior (depth) and craniocaudal (vertical) axes. The depth axis for the control heat map shows localised directional displacement on the inferior part of the caudate. This localised asymmetry is also evident in the FAS group but to a lesser degree, but is absent in the HEs. A vertical axis comparison shows control growth in a localised region of the superior part of the left caudate compared to the right which is absent in exposed groups. It should be noted that the asymmetry index refers to the magnitude of asymmetry, whereas mapping the original-reflected displacement shows the mean direction of asymmetry across the group. Thus, while the mean asymmetry index of HEs is comparable with controls, we do not see the same distinctive directional asymmetry in Fig 9, indicating this asymmetry is heterogeneous and not one-sided.

Caudate Asymmetry Correlations with Neurocognitive Performance in Prenatal Alcohol Exposure

We have shown how the exposed population expresses less asymmetry of the caudate compared to controls. Building a DSM including only individuals with PAE (FAS n=22; HE n=54) showed numerous correlations between PCs reflecting left-right caudate asymmetry and neurocognitive variables. However, reliance on correlations with individual PCs is not sufficiently robust for asymmetry analysis. Instead, we test the asymmetry-cognition relationship by computing 2-tailed Pearson correlation coefficients for correlations between

the caudate asymmetry indices, and each of the age-adjusted variables of the CVLT-C and DAS-2 tests. Results indicated significant correlations between asymmetry indices and age-adjusted z-scores for CVLT-C tests: discriminability (r2=0.15, p=0.011); long delayed cued recall (r2=0.11, p=0.029) and short delay cued recall (r2=0.13, p=0.027). Testing DAS-2 standardised scores and caudate asymmetry index revealed the same patterns of significant correlations for: general cognitive ability (GCA) (r2=0.1, p=0.036); spatial ability (r2=0.09, p=0.045); recall of designs (r2=0.1, p=0.034); sequential and quantitative reasoning ability score (r2=0.11, p=0.024); and verbal similarities ability score (r2=0.13, p=0.017). No such correlations existed in the control population on any of the neurocognitive test variables. See supplementary Fig S6 showing plotted correlations, table S2 for cohort characteristics of these neurocognitive variables and tables S3 and S4 for an explanation of CVLT-C and DAS-2 test outcomes.

DISCUSSION

A previous study of face-brain relationships in a murine model of prenatal alcohol exposure (Lipinski et al. 2012) used a DSM approach to analyse face and brain shape simultaneously. The face and brain components were segmented simultaneously from MRI volumes and thus could be processed in a single DSM model. In theory, this is possible with MRI volumes of the human head but the pads used to restrict head movement distort the soft tissues of the face. Therefore, in this study, we used an existing dataset of high-resolution facial images acquired with 3D stereophotogrammetry and segmented structural MRI images from 3T scanners of the same individuals and employed separate face and a brain surface representations to produce a series of combined models, each with a single set of PCA outputs. The resulting models represent the morphometric covariation of each brain component and the facial region linked statistically by a series of amalgamated principal component (PC) values. Additionally, we focus not only on the whole face but specific areas, which in FASDs are shown to have greater diagnostic significance. Previous DSM studies (Chinthapalli et al., 2012; Hammond et al., 2012a, 2005; Suttie et al., 2013) have shown the discriminating power of using only localised regions of the face.

Previous studies have focused on face-brain relationships that exist in PAE (Roussotte, 2012; Yang et al., 2012a). Yang and colleagues investigated the relationship between structural abnormalities of the corpus callosum from MRI images, and facial dysmorphology measures observed by specialist clinicians. 82 FASD and 71 non-exposed child and adolescent subjects were recruited from 2 sites in the USA and one in the Western Cape, South Africa. Surface-based measurements estimated localized corpus callosum thickness and area showing significant correlations with PFL in the FASD subset, however, no correlation was found between lipometer scores and corpus callosum measures. In addition, this study observed significant positive correlations between FSIQ and total area, the area of the isthmus, and areas of the anterior third of the corpus callosum. Although not stated in the results, our study did attempt to link corpus callosum morphology with neurocognitive outcome. We found PCs representing shape morphology produced from DSMs of the corpus callosum to correlate significantly with measures of cognitive performance in the FASD subjects. However, as these values are produced from PCA shape models they do not explicitly represent specific localised shape difference, and therefore not robust enough for

the analysis of brain-behavior relationships. However, similar to Yang et al., 2012a, our study demonstrates the relationships that exist between face and brain by combining localised regions of facial morphology with the corpus callosum. In addition, we include morphology of facial regions which are difficult for objective measurement, and not taken into account in routine FASD diagnostic examinations where only cardinal features (reduced PFL, philtrum smoothness, thinness of the upper lip vermillion) are prioritized for diagnosis.

In this analysis, midline facial regions (profile, philtrum, nose and upper-lip vermilion) and non-midline regions (face, eyes, mandible and malar) combined with the corpus callosum, and caudate nucleus in some instances, is more concordant with clinical classification for a control-FAS dichotomy. Midline facial regions combined with a midsagittal representation of the corpus callosum performed better the non-midline facial regions, improving control-FAS classification testing when compared to single structure models. Combining the caudate nucleus with the face did not improve classification accuracy, but when dividing the structure into its respective left-right halves, we determined noteworthy improvements using the left caudate combined with all regions except the nose. In all combined testing, we demonstrated that both brain structures improve control-FAS classification accuracy when combined with the lip-vermillion.

Exposed populations show a significant reduction in bilateral caudate nucleus volume as a proportional decrease relative to intracranial volume (Archibald et al., 2001; Astley et al., 2009; Joseph et al., 2014). It is evident from our PC1 representations and calculated volumes of the caudate nucleus that growth is diminished in exposed populations. However, our models do not control for total intracranial volume. As reported in the literature, the corpus callosum does not show consistent volume change with age (Pfefferbaum et al., 2013). Likewise in our analysis, growth trajectories from PC values did not correspond with the associated face-age trajectory (Suttie et al. 2013).

Given that the combined classification testing for left and right caudate differed so much it is fair to hypothesise left-right asymmetry differences between FAS and control groups. Using a methodology previously utilised in DSM studies of facial asymmetry in Autism Spectrum Disorders (Hammond et al., 2008) and the effects of different cancer treatment strategies (Schoot et al., 2017), we calculated measures of asymmetry for the caudate nucleus which on average shows control caudate nucleus to be more asymmetric compared to the FAS group. This is not the case for the HE subset, which shows no significant asymmetry index difference from controls. An axial displacement heat map showing directional asymmetry along a depth axis shows a left anterior dominance in controls and similarly in the FAS group but to a much lesser extent. In the HE group, directional asymmetry is inconclusive, indicating heterogeneous asymmetry across the group. Interestingly, lower asymmetry in the caudate of the PAE group was significantly correlated with lower neurocognitive performance. Several measures from the CVLT-C memory test and the DAS-2 general cognitive test significantly correlated with the caudate asymmetry index value. This finding supports the notion that brain-behaviour relationships exist in the particularly vulnerable structures in individuals with PAE. More specifically, asymmetry of the caudate appears to be strongly associated with general cognitive ability, verbal learning and recall in those with PAE. Previous studies have also identified brain-behaviour relationships that exist in

children with a history of PAE (Coles et al., 2011; Fryer et al., 2012; Gross et al., 2017; Roussotte, 2012), however, these are typically based on volumetric reductions. Fryer and colleagues observed that the most consistent, and significant associations were recorded for the bilateral volume of the caudate nucleus with all cognitive variables recorded. This remained a significant predictor of cognitive performance, even after accounting for confounding variables (total brain volume, IQ, and age).

In a previous study, Sowell et al. 2002 reported individuals with PAE to have reduced asymmetry of the cortical surface and grey matter density compared to controls, indicating that the development of typical brain asymmetry can be lost in exposed populations. As craniofacial and neural development are intrinsically linked, it seems natural for asymmetry of one to be reflected in the other. However, contrary to our findings and those of Sowell et al., a study of facial asymmetry (Klingenberg et al., 2010) observed significant differences in directional asymmetry of individuals with a FAS diagnosis compared to controls, in both a Finnish and a South African population. In this landmark based study, average directional asymmetry was identified as a midline landmark shift to the right and of the eyes to the left. In our study of the caudate nucleus, it is perhaps the deep location of this structure within the brain that disengages its relationship with the midline of the face. There is a higher likelihood that asymmetry of the brain will influence or co-occur with that of the face when regions of focus are directly adjacent (Hammond et al., 2008).

Previous studies of the caudate nuclei, with mention of left-right differences, predominantly focus on volumetric asymmetry (Archibald et al., 2001; Astley et al., 2009; Fryer et al., 2012; Hynd et al., 1993; Nardelli et al., 2011; O'Dwyer et al., 2016; Willford et al., 2010). Willford et al. produced a study focusing on asymmetry of the caudate nucleus in offspring of mothers who drank alcohol in moderate quantities during pregnancy. A population of young adults (n=45; 18–22yrs) were recruited for this MRI study and separated into 3 groups based on their trimester dependent prenatal alcohol exposure: controls (no alcohol exposure, n=20); 1T (first trimester only exposure, n=15); and, 3T (exposure throughout all three trimesters, n=10). The authors calculated the magnitude of asymmetry by subtracting the left caudate volume with the right and dividing by the total ([L-R]/[L+R]). The resulting analysis found dose-dependent effects with the 3T groups showing a statistically significant leftward bias in caudate asymmetry compared to 0T, with the 1T group being an intermediate between the 0T and 3T groups but statistically non-significant compared to either. Additionally, this study controlled for tobacco and marijuana use concluding that neither of these significantly affect caudate volume or asymmetry. Although this study was thorough in controlling for influencing factors, results were limited by small sample size reducing the statistical power.

That only the FAS group demonstrated a significant, and more consistently reduced left-right caudate nucleus asymmetry compared to controls is most likely due to the fact, that to create the craniofacial features of FAS, alcohol exposure must occur in the 3rd-4th weeks of human development. At this stage, the tissues that will make up the brain and face are still developing as a single structure, which is why craniofacial dysmorphology frequently accompanies striatal and other rostral midline brain structure abnormalities (Donald et al., 2015; Godin et al., 2011, 2010). The less consistent effects in the HE group suggests alcohol

exposure during later stages of development, demonstrating that while the severe craniofacial effects in FAS children largely result from prenatal alcohol exposure in a narrow time window, while the caudate nucleus (and many other regions of the brain) are susceptible over a much wider period. The fact that ethanol exposure seems to have a more significant effect on the left caudate nucleus has also been observed in a mouse model of early gestational alcohol exposure, where both sides of the caudate nucleus was affected, but there appears to be a slight leftward bias, possibly due to the differential left-right sonic hedgehog (Shh) concentration gradients present in early embryos (Fish et al., 2016).

Determining correlations between localised facial region, structural brain anomalies and cognitive outcomes is important as it could ultimately provide insight for clinicians to determine the extent of neuro-structural damage by morphometric analysis of the face. This study has focused on two regions known to be disproportionally affected by alcohol teratogenesis and future studies should apply DSM analysis to lesser affected brain structures to determine if subtle face-brain relationships are present and if further brain-behaviour associations can be supported. It is important to emphasise that MRI image analysis is highly unlikely ever to be part of the routine diagnosis of FASDs. However, its use in face-brain analysis might help identify subtle facial dysmorphism associated with neurological pathologies in FASD individuals, particularly the HE population where recognition of facial effects is challenging for even experienced clinicians.

Supplementary Material

Refer to Web version on PubMed Central for supplementary material.

Acknowledgments

Sources of Support:

This international collaborative study was completed in conjunction with the Collaborative Initiative on Fetal Alcohol Spectrum Disorders (CIFASD) and is funded by NIH/National Institute on Alcohol Abuse and Alcoholism: U01AA014809 (to T.F. and P.H.); U24AA014815 (to K.L.J.); U01014834 (to S.M.); U01AA017122 (to E.R.S.); U24AA014811 (E.P.R.); Additional information about CIFASD can be found at www.cifasd.org.

Abbreviations:

ATL	Atlanta
CC	corpus callosum
CDSM	combined dense surface model
CI	confidence interval
CIFASD	The Collaborative Initiative on Fetal Alcohol Spectrum Disorders
CM	closest mean
CN	caudate nucleus
CNS	central nervous system

CVLT-C	California Verbal Learning Test, Children's Edition
DAS-2	Differential Ability Scales-Second Edition
DSM	dense surface model
FAS	fetal alcohol syndrome
FASD	fetal alcohol spectrum disorder
FOV	field of view
HE	heavy alcohol exposure but not diagnosable clinically as FAS
LA	Los Angeles
LDA	linear discriminant analysis
MN	Minneapolis
PAE	prenataly alcohol exposed
PFL	palpebral fissure length
PC	principal component
ROC	receiver operating curves
SD	San Diego
SVM	support vector machines
Shh	sonic hedgehog
TE	echo time
TR	repetition time

REFERENCES

Archibald SL, Fennema-Notestine C, Gamst A, Riley EP, Mattson SN, Jernigan TL (2001) Brain dysmorphology in individuals with severe prenatal alcohol exposure. Dev Med Child Neurol 43:148–54. [PubMed: 11263683]

Astley SJ, Aylward EH, Olson HC, Kerns K, Brooks A, Coggins TE, Davies J, Dorn S, Gendler B, Jirikowic T, Kraegel P, Maravilla K, Richards T (2009) Magnetic resonance imaging outcomes from a comprehensive magnetic resonance study of children with fetal alcohol spectrum disorders. Alcohol Clin Exp Res 33:1671–89. [PubMed: 19572986]

Astley SJ, Clarren SK (2001) Measuring the facial phenotype of individuals with prenatal alcohol exposure: correlations with brain dysfunction. Alcohol Alcohol 36:147–59. [PubMed: 11259212]

Bookstein FL (1997) Shape and the Information in Medical Images: A Decade of the Morphometric Synthesis. Comput Vis Image Underst 66:97–118.

Bookstein FL, Connor PD, Huggins JE, Barr HM, Pimentel KD, Streissguth AP (2007) Many infants prenatally exposed to high levels of alcohol show one particular anomaly of the corpus callosum. Alcohol Clin Exp Res 31:868–79. [PubMed: 17386071]

Chinthapalli K, Bartolini E, Novy J, Suttie M, Marini C, Falchi M, Fox Z, Clayton LMS, Sander JW, Guerrini R, Depondt C, Hennekam R, Hammond P, Sisodiya SM (2012) Atypical face shape and genomic structural variants in epilepsy. Brain.

Chudley A, Conry J, Cook J, Loock C, Rosales T, LeBlanc N (2005) Fetal alcohol spectrum disorder: Canadian guidelines for diagnosis. Can Med Assoc J 172:S1–S21. [PubMed: 15738468]

Coles CD, Goldstein FC, Lynch ME, Chen X, Kable JA, Johnson KC, Hu X (2011) Memory and brain volume in adults prenatally exposed to alcohol. Brain Cogn 75:67–77. [PubMed: 21067853]

Cox-Brinkman J, Vedder A, Hollak C, Richfield L, Mehta A, Orteu K, Wijburg F, Hammond P (2007) Three-dimensional face shape in Fabry disease. Eur J Hum Genet 15:535–542. [PubMed: 17327876]

Delis DC, Kramer JH, Kaplan E, Ober BA (1994) California Verbal Learning Test®—Children's Version (CVLT®–C). San Antonio, TX Psychol Corp.

Donald KA, Eastman E, Howells FM, Adnams C, Riley EP, Woods RP, Narr KL, Stein DJ (2015) Neuroimaging effects of prenatal alcohol exposure on the developing human brain: a magnetic resonance imaging review. Acta Neuropsychiatr 1–19.

Elliott C (2007) Differential Ability Scales (2nd ed.). San Antonio, TX Harcourt Assess.

Ellson J, Gansber E, Koutsofios L, North S, Woodhull GL (2002) Graphviz- Open Source Graph Drawing Tools. Berlin Heidelberg, Ger Springer-Verlag Berlin Heidelberg; 594–597.

Fish EW, Holloway HT, Rumple A, Baker LK, Wieczorek LA, Moy S., Paniagua B, Parnell SE (2016) Acute alcohol exposure during neurulation: Behavioral and brain structural consequences in adolescent C57BL/6J mice. Behav Brain Res 311:70–80. [PubMed: 27185739]

Fryer SL, Mattson SN, Jernigan TL, Archibald SL, Jones KL, Riley EP (2012) Caudate Volume Predicts Neurocognitive Performance in Youth with Heavy Prenatal Alcohol Exposure. Alcohol Clin Exp Res 36:1932–1941. [PubMed: 22551091]

Godin EA, Dehart DB, Parnell SE, O'Leary-Moore SK, Sulik KK (2011) Ventromedian forebrain dysgenesis follows early prenatal ethanol exposure in mice. Neurotoxicol Teratol 33:231–239. [PubMed: 21074610]

Godin EA, O'Leary-Moore SK, Khan AA, Parnell SE, Ament JJ, Dehart DB, Johnson BW, Allan Johnson G, Styner MA, Sulik KK (2010) Magnetic Resonance Microscopy Defines Ethanol-Induced Brain Abnormalities in Prenatal Mice: Effects of Acute Insult on Gestational Day 7. Alcohol Clin Exp Res 34:98–111. [PubMed: 19860813]

Gross LA, Moore EM, Wozniak JR, Coles CD, Kable JA, Sowell ER, Jones KL, Riley EP, Mattson SN (2017) Neural correlates of verbal memory in youth with heavy prenatal alcohol exposure. Brain Imaging Behav 1–17. [PubMed: 26780240]

Gwilliam JR, Cunningham SJ, Hutton T (2006) Reproducibility of soft tissue landmarks on three-dimensional facial scans. Eur J Orthod 28:408–415. [PubMed: 16901962]

Hammond P, Forster-Gibson C, Chudley A E, Allanson JE, Hutton TJ, Farrell S a, McKenzie J, Holden JJ a, Lewis MES (2008) Face-brain asymmetry in autism spectrum disorders. Mol Psychiatry 13:614–23. [PubMed: 18317467]

Hammond P, Hannes F, Suttie M, Devriendt K, Vermeesch JR, Faravelli F, Forzano F, Parekh S, Williams S, McMullan D, South ST, Carey JC, Quarrell O (2012a) Fine-grained facial phenotype-genotype analysis in Wolf-Hirschhorn syndrome. Eur J Hum Genet 20:33–40. [PubMed: 21792232]

Hammond P, Hutton TJ, Allanson JE, Buxton B, Campbell LE, Clayton-Smith J, Donnai D, Karmiloff-Smith A, Metcalfe K, Murphy KC, Patton M, Pober B, Prescott K, Scambler P, Shaw A, Smith ACM, Stevens AF, Temple IK, Hennekam R, Tassabehji M (2005) Discriminating power of localized three-dimensional facial morphology. Am J Hum Genet 77:999–1010. [PubMed: 16380911]

Hammond P, Suttie M (2012) Large-scale objective phenotyping of 3D facial morphology. Hum Mutat 33:817–25. [PubMed: 22434506]

Hammond P, Suttie M, Hennekam RC, Allanson J, Shore EM, Kaplan FS (2012b) The face signature of fibrodysplasia ossificans progressiva. Am J Med Genet Part A 158A:1368–1380. [PubMed: 22581580]

Hennessy RJ, McLearie S, Kinsella A, Waddington JL (2005) Facial surface analysis by 3D laser scanning and geometric morphometrics in relation to sexual dimorphism in cerebral--craniofacial morphogenesis and cognitive function. J Anat 207:283–95. [PubMed: 16185253]

Heulens I, Suttie M, Postnov A, De Clerck N, Perrotta CS, Mattina T, Faravelli F, Forzano F, Kooy RF, Hammond P (2013) Craniofacial characteristics of fragile X syndrome in mouse and man. Eur J Hum Genet 21:816–23. [PubMed: 23211703]

Hoyme HE, Kalberg WO, Elliott A, Blankenship J, Buckley D, Marais A- S, B N, Manning M, Robinson LK, Chambers CD, Jones KL, Adnams C, Prachi S, Riley EP, Michael C, Kenneth W, May P a (2016) Updated Guidelines for Fetal Alcohol Spectrum Disorders. Pediatrics 138.

Hoyme HE, May P a, Kalberg WO, Kodituwakku P, Gossage JP, Trujillo PM, Buckley DG, Miller JH, Aragon AS, Khaole N, Viljoen DL, Jones KL, Robinson LK (2005) A practical clinical approach to diagnosis of fetal alcohol spectrum disorders: clarification of the 1996 institute of medicine criteria. Pediatrics 115:39–47. [PubMed: 15629980]

Hynd GW, Hern KL, Novey ES, Eliopulos D, Marshall R, Gonzalez JJ, Voeller KK (1993) Attention Deficit- Hyperactivity Disorder and Asymmetry of the Caudate Nucleus. J Child Neurol 8:339–347. [PubMed: 8228029]

Jenkinson M, Beckmann CF, Behrens TEJ, Woolrich MW, Smith SM (2012) FSL. Neuroimage 62:782–90. [PubMed: 21979382]

Jones KL, Hoyme HE, Robinson LK, Del Campo M, Manning M a, Prewitt LM, Chambers CD (2010) Fetal alcohol spectrum disorders: Extending the range of structural defects. Am J Med Genet A 152A:2731–5. [PubMed: 20949507]

Jorge Cardoso M, Leung K, Modat M, Keihaninejad S, Cash D, Barnes J, Fox NC, Ourselin S (2013) STEPS: Similarity and Truth Estimation for Propagated Segmentations and its application to hippocampal segmentation and brain parcelation. Med Image Anal 17:671–84. [PubMed: 23510558]

Joseph J, Warton C, Jacobson SW, Jacobson JL, Molteno CD, Eicher A, Marais P, Phillips OR, Narr KL, Meintjes EM (2014) Three-dimensional surface deformation-based shape analysis of hippocampus and caudate nucleus in children with fetal alcohol spectrum disorders. Hum Brain Mapp 35:659–72. [PubMed: 23124690]

Klingenberg CP, Barluenga M, Meyer A (2002) Shape analysis of symmetric structures: Quantifying variation among individuals and asymmetry. Evolution (N Y) 56:1909–1920.

Klingenberg CP, Wetherill L, Rogers J, Moore E, Ward R, Autti-Rämö I, Fagerlund a, Jacobson SW, Robinson LK, Hoyme HE, Mattson SN, Li TK, Riley EP, Foroud T (2010) Prenatal alcohol exposure alters the patterns of facial asymmetry. Alcohol 44.

Lipinski R, Hammond P, O'Leary-Moore SK, Ament JJ, Pecevich SJ, Jiang Y, Budin F, Parnell SE, Suttie M, Godin E a., Everson JL, Dehart DB, Oguz I, Holloway HT, Styner M a., Johnson GA, Sulik KK (2012) Ethanol-induced face-brain dysmorphology patterns are correlative and exposure-stage dependent. PLoS One 7:e43067. [PubMed: 22937012]

Mattson SN, Crocker N, Nguyen TT (2011) Fetal Alcohol Spectrum Disorders: Neuropsychological and Behavioral Features. Neuropsychol Rev 21:81–101. [PubMed: 21503685]

May P a, Brooke L, Gossage JP, Croxford J, Adnams C, Jones KL, Robinson L, Viljoen D (2000) Epidemiology of fetal alcohol syndrome in a South African community in the Western Cape Province. Am J Public Health 90:1905–12. [PubMed: 11111264]

McGee CL (2005) Fetal alcohol spectrum disorders: an overview with emphasis on changes in brain and behavior. Exp Biol Med (Maywood) 230:357–365.

Modat M, Ridgway GR, Taylor ZA, Lehmann M, Barnes J, Hawkes DJ, Fox NC, Ourselin S (2010) Fast free-form deformation using graphics processing units. Comput Methods Programs Biomed 98:278–284. [PubMed: 19818524]

Nardelli A, Lebel C, Rasmussen C, Andrew G, Beaulieu C (2011) Extensive deep gray matter volume reductions in children and adolescents with fetal alcohol spectrum disorders. Alcohol Clin Exp Res 35:1404–17. [PubMed: 21575012]

O'Dwyer L, Tanner C, Van Dongen E V., Greven CU, Bralten J, Zwiers MP, Franke B, Heslenfeld D, Oosterlaan J, Hoekstra PJ, Hartman CA, Groen W, Rommelse N, Buitelaar JK (2016) Decreased

left caudate volume is associated with increased severity of autistic-like symptoms in a cohort of ADHD patients and their unaffected siblings. PLoS One 11:1–20.

Ourselin S, Roche A, Prima S, Ayache N (2000) Block Matching: A General Framework to Improve Robustness of Rigid Registration of Medical Images In: Medical Image Computing and Computer-Assisted Intervention -- MICCAI 2000: Third International Conference, Pittsburgh, PA, USA, 10 11–14, 2000 Proceedings (Delp SL, DiGoia AM, Jaramaz B eds), pp 557–566. Berlin, Heidelberg, Springer Berlin Heidelberg.

Pfefferbaum A, Rohlfing T, Rosenbloom MJ, Chu W, Colrain IM, Sullivan E V. (2013) Variation in longitudinal trajectories of regional brain volumes of healthy men and women (ages 10 to 85years) measured with atlas-based parcellation of MRI. Neuroimage 65:176–193. [PubMed: 23063452]

Postema FA, Hopman SM, de Borgie CA, Hammond P, Hennekam RC, Merks JH, Tu PS s g, Aalfs CM, Anninga JK, Berger LP, Bleeker FE, de Bont ES, de Borgie CA, Dommering CJ, van Eijkelenburg NK, Hammond P, Hennekam RC, van den Heuvel-Eibrink MM, Hopman SM, Jongmans MC, Kors WA, Letteboer TG, Loeffen JL, Merks JH, Olderode-Berends MJ, Postema FA, Wagner A, Tu PS s g (2017) Validation of a clinical screening instrument for tumour predisposition syndromes in patients with childhood cancer (TuPS): protocol for a prospective, observational, multicentre study. BMJ Open 7:e013237.

Riley EP, Mattson SN, Sowell ER, Jernigan TL, Sobel DF, Jones KL (1995) Abnormalities of the corpus callosum in children prenatally exposed to alcohol. Alcohol Clin Exp Res 19:1198–202. [PubMed: 8561290]

Roussotte F (2012) Regional brain volume reductions relate to facial dysmophology and neurocognitive function in fetal alcohol spectrum disorders. Hum Brain Mapp 33.

Schoot RA, Hol MLF, Merks JHM, Suttie M, Slater O, van Lennep M, Hopman SMJ, Dunaway D, Syme-Grant J, Smeele LE, Zwinderman KH, Caron HN, Hammond P (2017) Facial asymmetry in head and neck rhabdomyosarcoma survivors. Pediatr Blood Cancer 64:1–8.

Sowell E (2002) Mapping Cortical Gray Matter Asymmetry Patterns in Adolescents with Heavy Prenatal Alcohol Exposure. Neuroimage 17:1807–1819. [PubMed: 12498754]

Sowell ER, Mattson SN, Thompson PM, Jernigan TL, Riley EP, Toga AW (2001) Mapping callosal morphology and cognitive correlates: Effects of heavy prenatal alcohol exposure. Neurology 57:235–244. [PubMed: 11468307]

Suttie M, Foroud T, Wetherill L, Jacobson JL, Molteno CD, Meintjes EM, Hoyme HE, Khaole N, Robinson LK, Riley EP, Jacobson SW, Hammond P (2013) Facial dysmorphism across the fetal alcohol spectrum. Pediatrics 131:e779-88. [PubMed: 23439907]

Suttie M, Wetherill L, Jacobson SW, Jacobson JL, Hoyme HE, Sowell ER, Coles C, Wozniak JR, Riley EP, Jones KL, Foroud T, Hammond P (2017) Facial Curvature Detects and Explicates Ethnic Differences in Effects of Prenatal Alcohol Exposure. Alcohol Clin Exp Res 1–13.

Willford J, Day R, Aizenstein H, Day N (2010) Caudate asymmetry: A neurobiological marker of moderate prenatal alcohol exposure in young adults. Neurotoxicol Teratol 32:589–594. [PubMed: 20609385]

Yang Y, Phillips OR, Kan E, Sulik KK, Mattson SN, Riley EP, Jones KL, Adnams CM, May P a, O'Connor MJ, Narr KL, Sowell ER (2012a) Callosal thickness reductions relate to facial dysmorphology in fetal alcohol spectrum disorders. Alcohol Clin Exp Res 36:798–806. [PubMed: 22150665]

Yang Y, Roussotte F, Kan E, Sulik KK, Mattson SN, Riley EP, Jones KL, Adnams CM, May P a, O'Connor MJ, Narr KL, Sowell ER (2012b) Abnormal cortical thickness alterations in fetal alcohol spectrum disorders and their relationships with facial dysmorphology. Cereb Cortex 22:1170–9. [PubMed: 21799209]

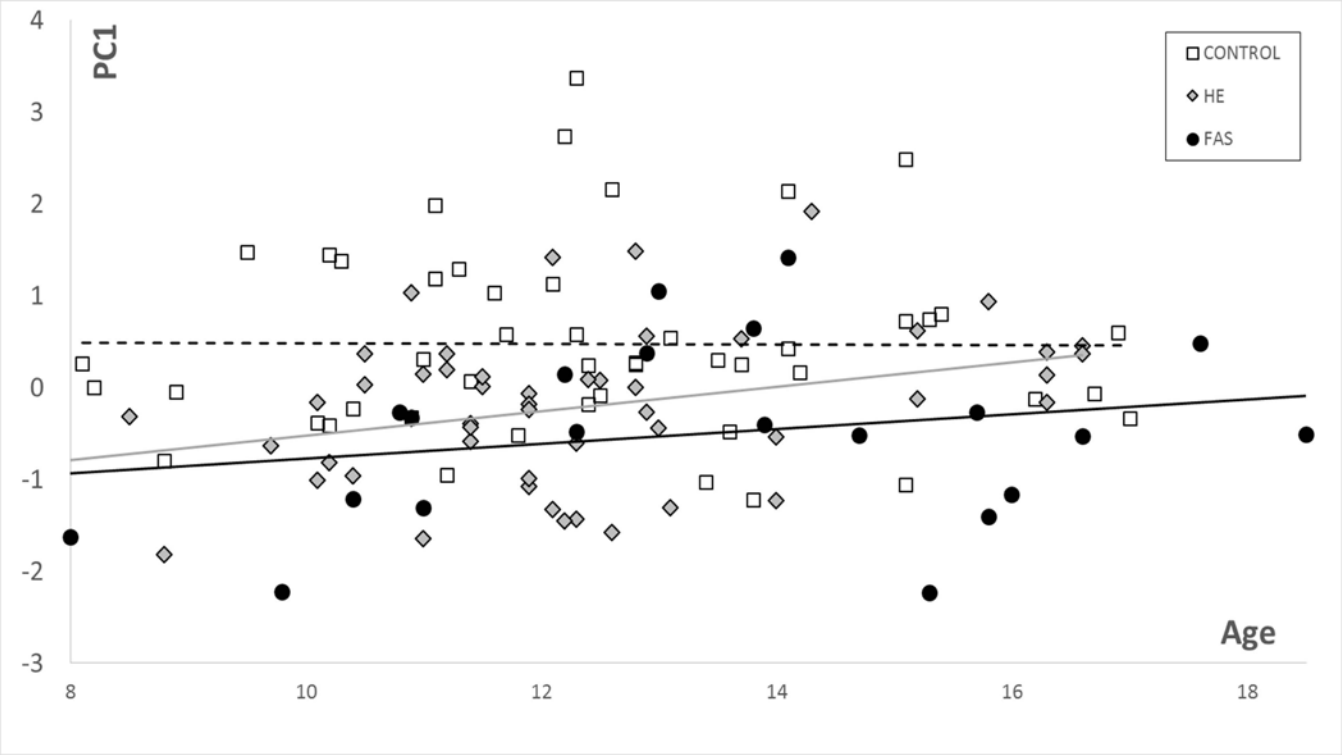

Figure 1.
PC1 vs age for corpus callosum suggests reduced growth for FAS (P<0.00001) and HE (P<0.03) compared to controls.

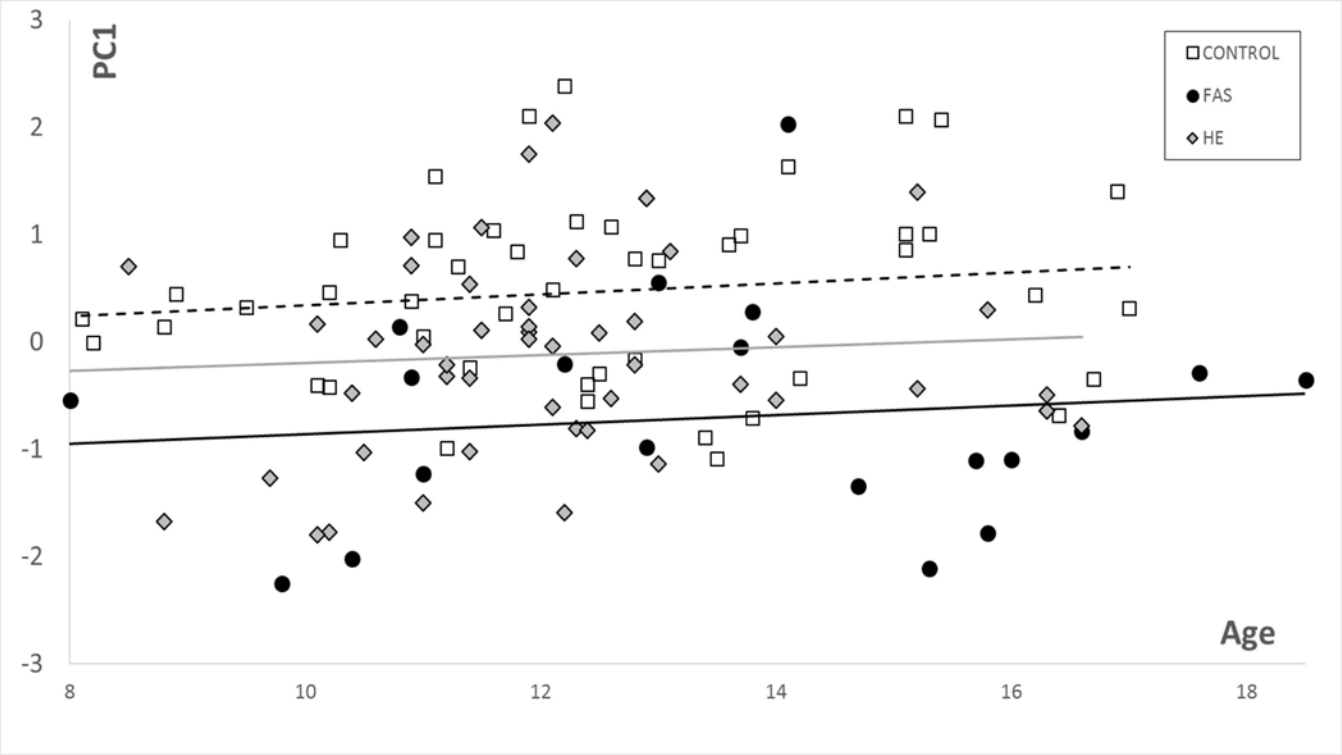

Figure 2.
PC1 vs age for caudate nucleus suggests reduced growth for FAS (P<0.00001) and HE (P<0.002) compared to controls.

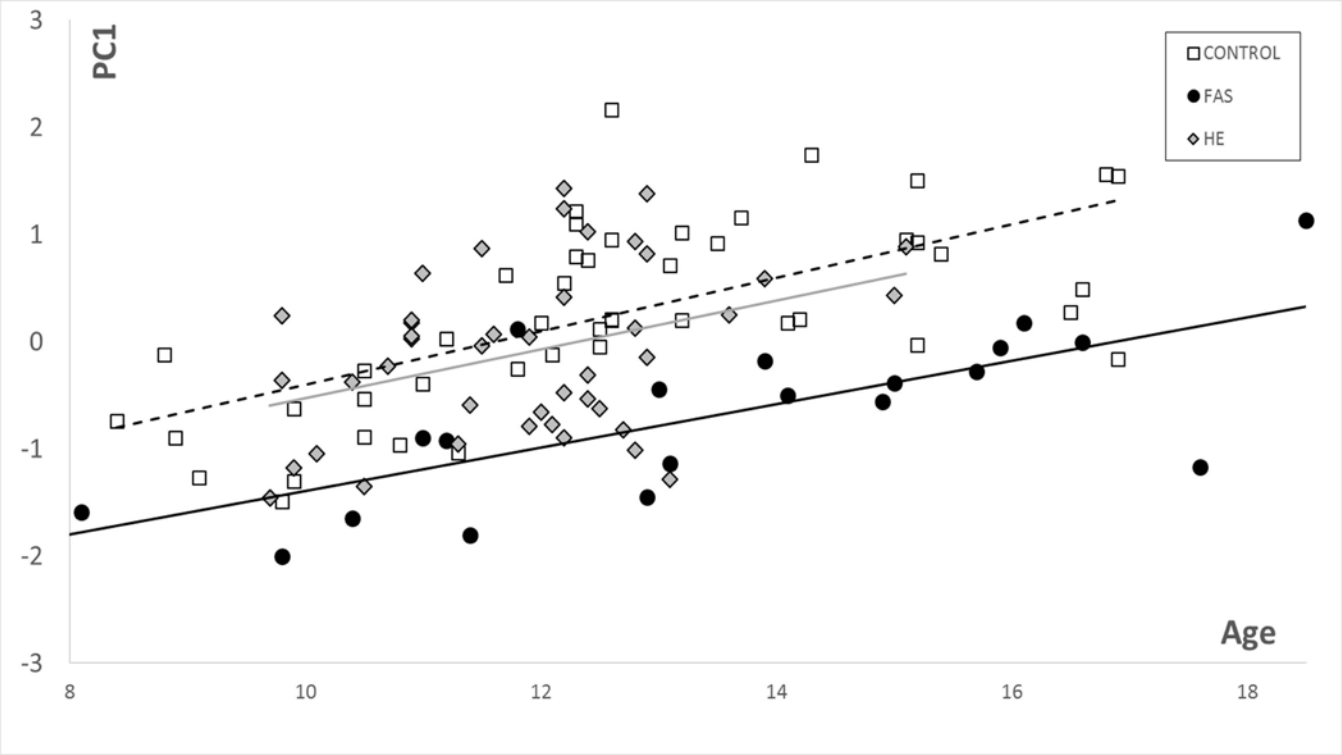

Figure 3.
PC1 vs age for face, suggesting reduced growth for FAS (P<0.0001) and marginally lower for HE (P<0.06).

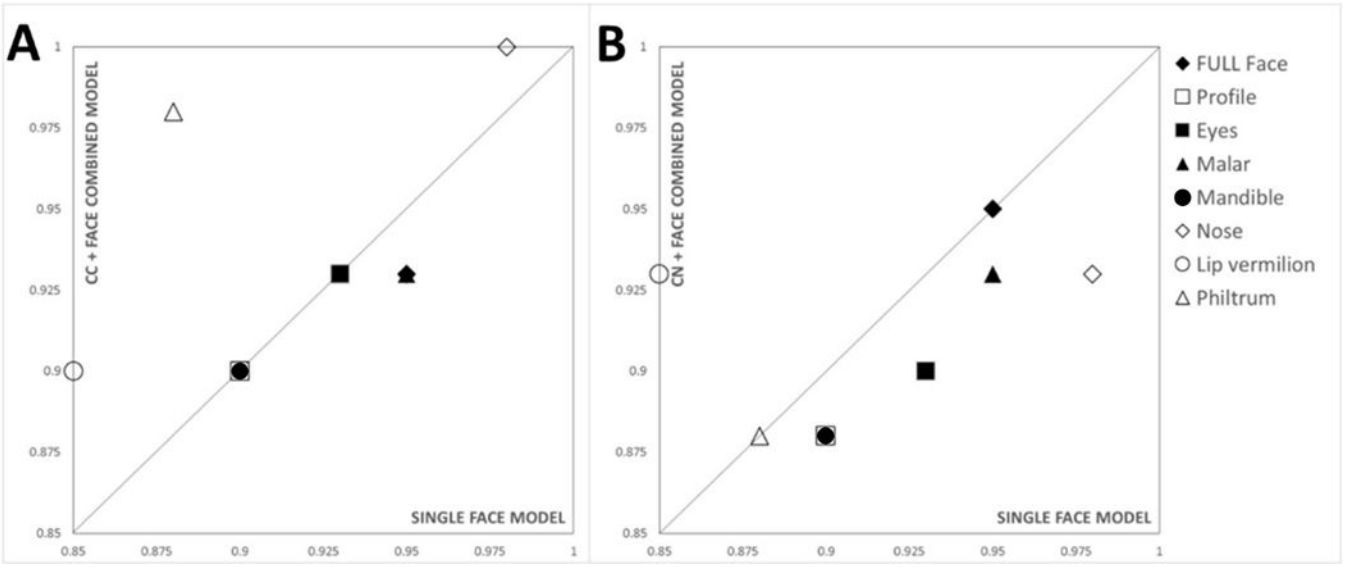

Figure 4.

Discrimination rates for face only (X-axis) vs face-brain (Y-axis) for A) corpus callosum and B) the caudate nucleus (whole). Midline facial structures (nose, lip vermillion, profile and philtrum) are labelled with unfilled symbols, and non-midline structures (full face, eyes, malar and mandible) by filled symbols. Compared to single model representations of face and brain, classification accuracy is increased when combining the corpus callosum with midline facial regions (nose (1.0), lip vermillion (0.90), philtrum (0.98)) but remains unchanged for profile (0.90). Combining the caudate nucleus with facial regions improved classification for lip vermillion (0.90) but not the mandible (0.90) or philtrum (0.98). All other face regions (eyes, mandible, profile, malar and nose) gave inferior classification results when combined with brain components.

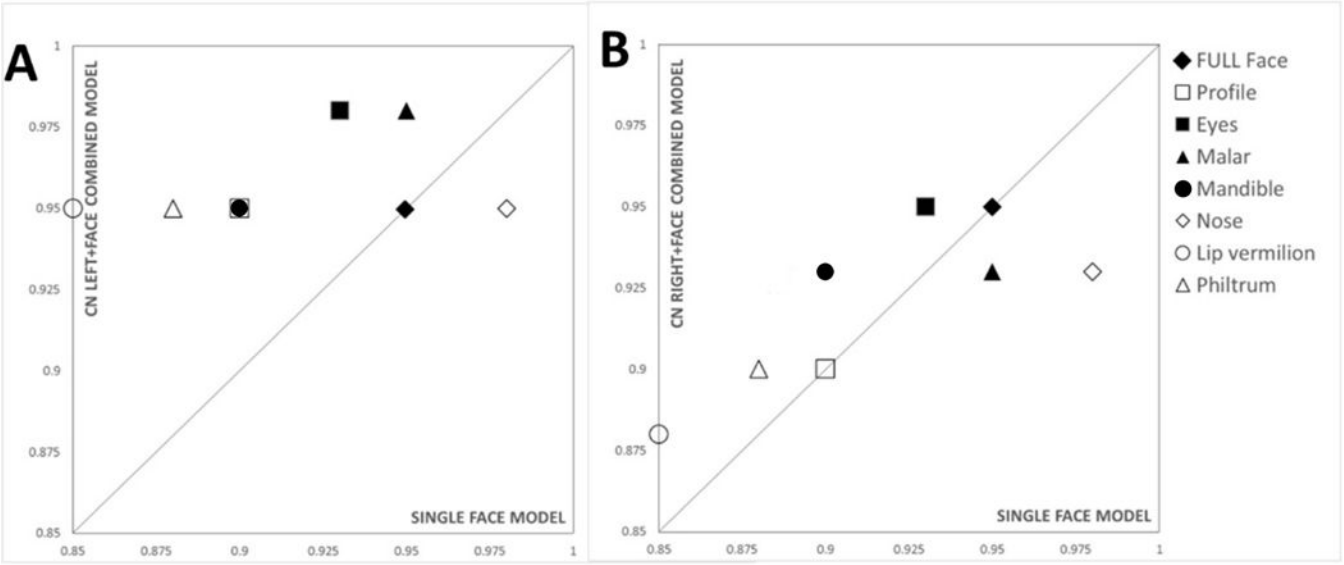

Figure 5.

Discrimination rates for face only (X-axis) vs combined face-brain (Y-axis) for A) left and B) right caudate nucleus. Midline facial structures (nose, lip vermillion, profile and philtrum) are labelled with unfilled symbols, and non-midline structures (full face, eyes, malar and mandible) represented by filled symbols. Compared to single model representations of face and brain, only moderate improvements were observed when combining right caudate nucleus with facial regions with the exception of nose and malar (B). In contrast, left caudate nucleus improved discrimination rates when combined with lip vermillion (0.95), malar (0.98), nose (0.95), eyes (0.98), profile (0.95) and remained unchanged for the full face (0.95). Face-brain classification for left or right caudate nucleus did not differ substantially for midline and non-midline facial regions.

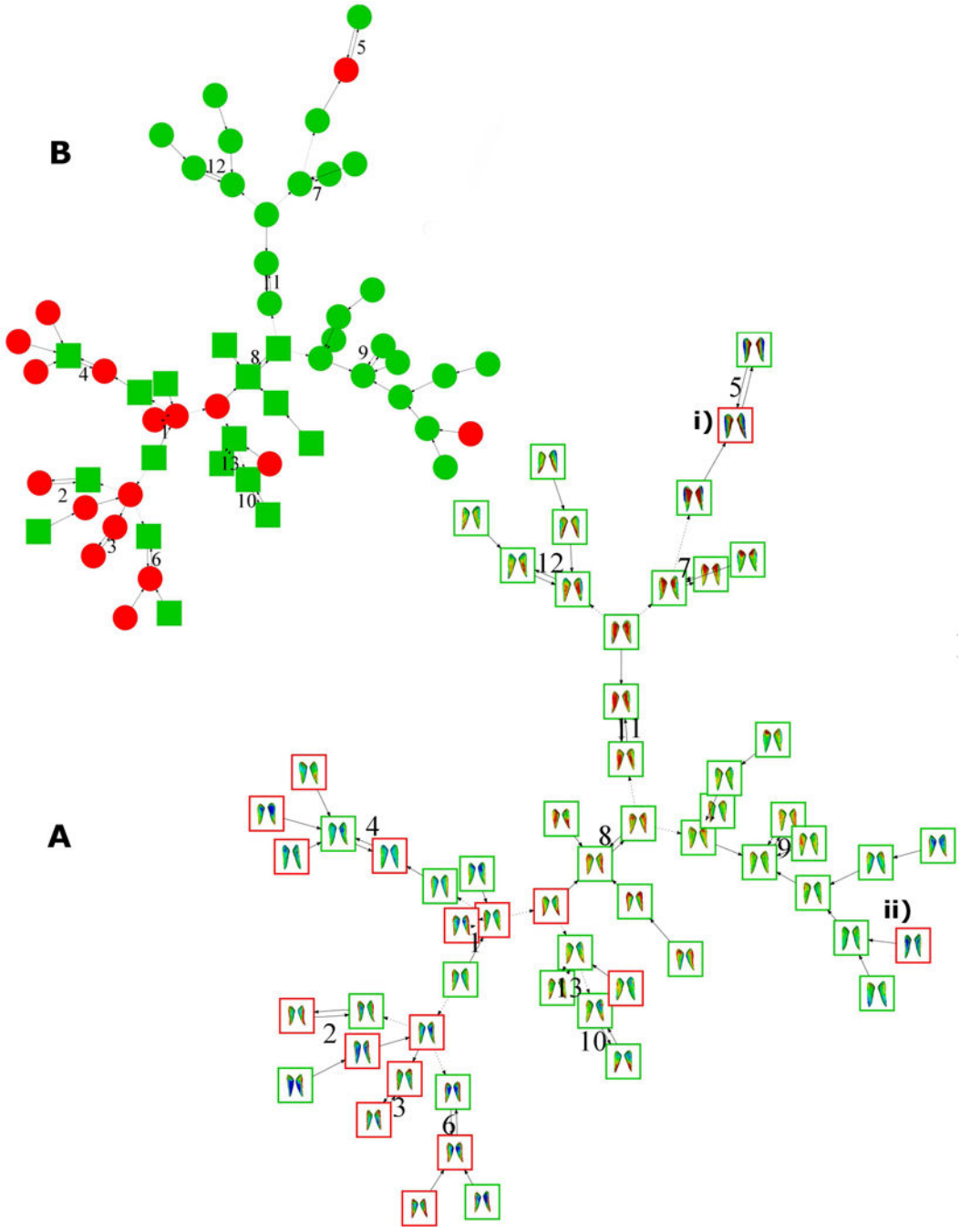

Figure 6.

Caudate nucleus signature graphs for 59 alcohol-exposed individuals colour coded as FAS (red, n=17) and HE (green, n=42). A) Graph is shown with caudate nucleus signatures showing a FAS-like subclustering of a subset of HE individuals 8. B) Colour coded binary representation with FAS-like HE nodes (green squared, n=17) and the remaining HEs (green circles, n=25) to illustrate the upper/lower graph ii are FAS outliers that do not cluster with other FAS individuals. A.i and A.ii show two FAS individuals in the 9th and 5th clusters who do not show affinity with the FAS group.

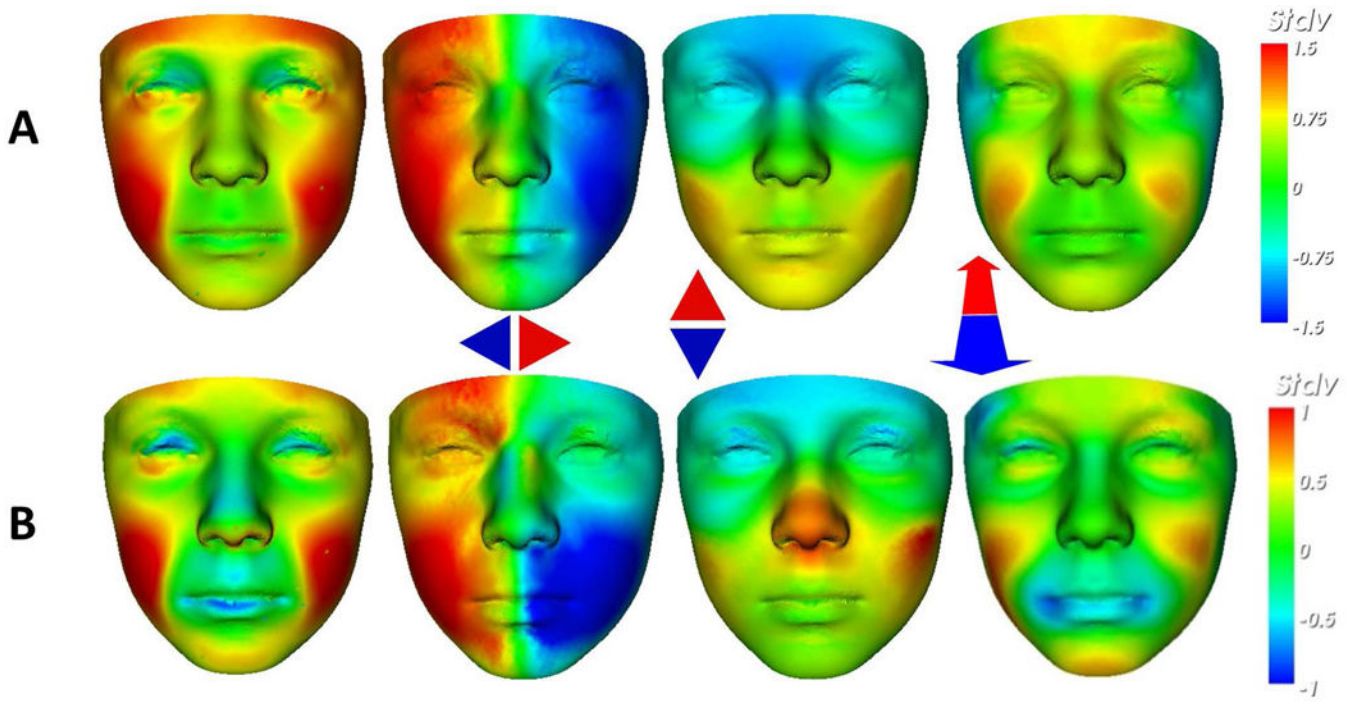

Figure 7.

Comparing mean facial signatures along each axis between A) FAS mean (n=22) at ±1.5SD and B) the FAS-like HE subset (n=17) at ±1SD induced in the caudate nucleus signature graph. This visualisation allows us to identify regions of similar dysmorphism; malar flattening (red in mid-face; cols 1 & 4); philtrum smoothness (faint blue on philtrum groove; col 1); retrognathia (red on the chin; col 4); overall size reduction (red in col 1 and lateral red-blue in col 2). The FAS-like partition on the horizontal axis (B, col 3) also shows shortening of nose (red on columella) which is a FAS-associated feature but is not visible in the equivalent FAS mean signature (A, col 3).

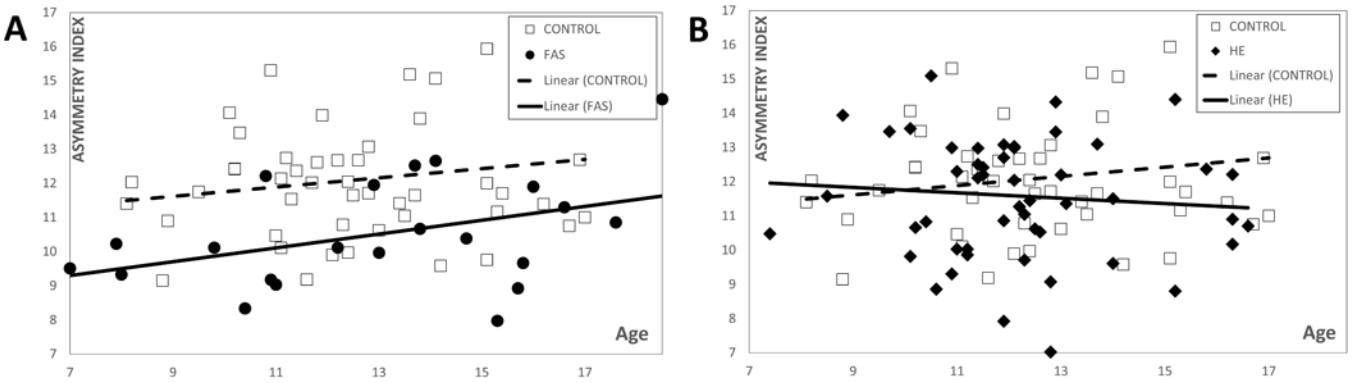

Figure 8.

Caudate nucleus asymmetry index (distance between DSM representations of caudate nucleus and its reflection) against age for A) FAS vs Control and B) HE vs Control. The control group has a significantly higher mean asymmetry index (12.1) compared to that (10.5) of the FAS group ($p<0.002$). In contrast, there is no significant difference between controls and HE.

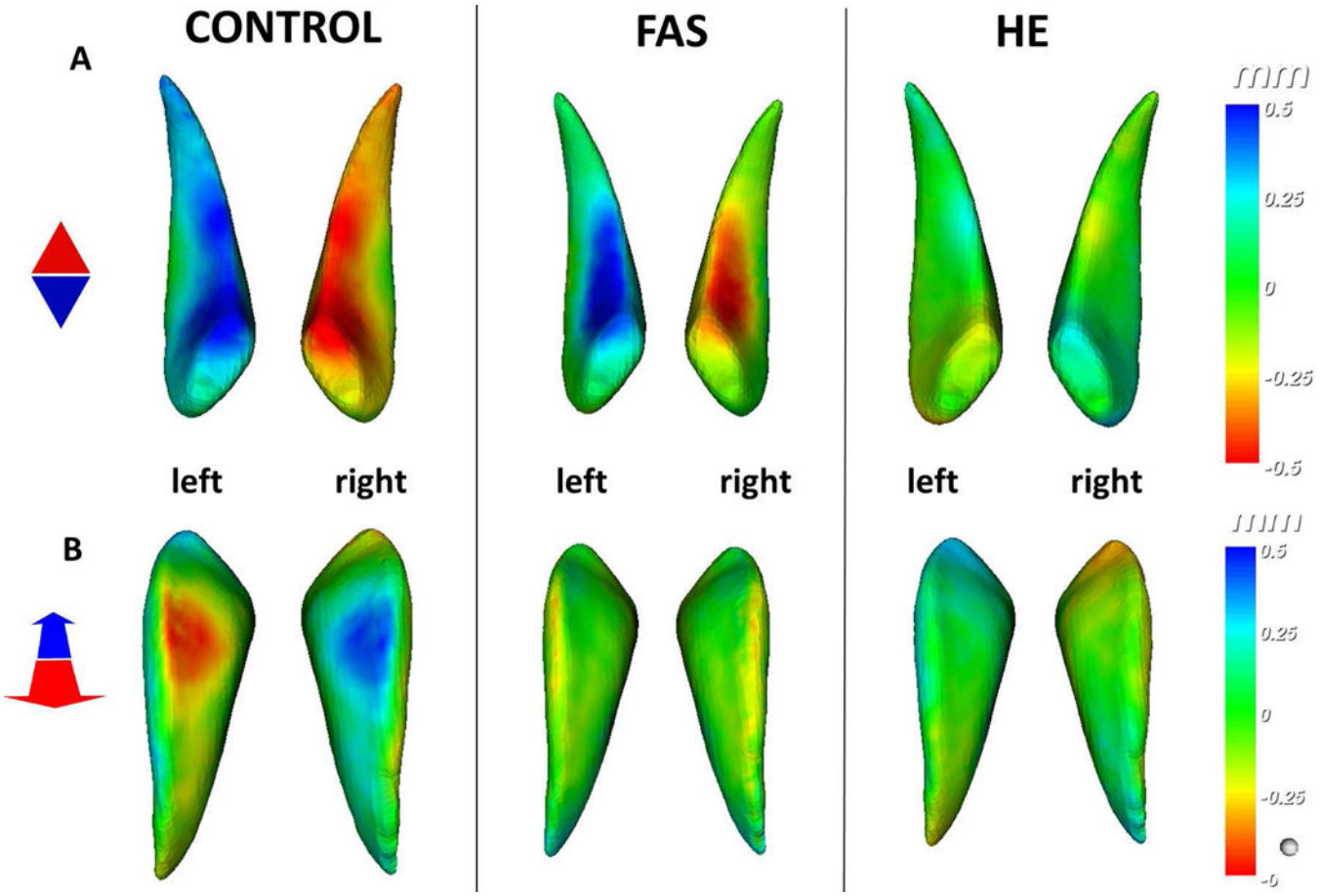

Figure 9.

Mean directional asymmetry represented by calculating displacement of mean original to mean reflected caudate nucleus for control, FAS and HE groups along A) anteroposterior (depth) and B) craniocaudal (vertical) axes ±0.5mm. A) Shows indication of a left anterior dominance in controls and similarly in FAS but to a lesser extent and localised. The HE mean at the same scale shows little to no mean left-right surface differences in that region indicating that asymmetry in the HE group is not homogenous. B) On a vertical axes we see localised dominance on the superior part of the left caudate, but FAS and HE means show no evidence of the same asymmetry.

Table 1.

Summary of the criteria used for categorising FAS (Hoyme et al. 2016), and the delineation from nonsyndromic HE children. FAS is diagnosed with or without exposure requiring 2 or more cardinal facial features, growth deficiency ≤10th percentile and the presence of a brain defect. The HE category does not necessitate traits other than excessive maternal alcohol intake (minimum 7oz absolute alcohol per week (≥14 standard drink measures) or occasional binges of 5 or more drinks.

	Criteria	FAS	HE
Alcohol exposure	Confirmed excessive gestational alcohol consumption	-	✓
Face	PFL (≤10th percentile) Thin upper lip (Astley scale 4 or 5) Smooth philtrum	≥2 of 3	
Growth	Height weight (≤10th percentile)	✓	
Brain defects	Head circumference (≤10th percentile) Structural abnormality (CNS)	≥1 of 2	
Neurobehavioral impairment	Behavioural or cognitive deficit	-	

Table 2.

Sample characteristics; values represent mean ± SD or %. *F* statistic is produced from single factor ANOVA testing. Dose-dependent relations for head circumference: FAS < HE and controls (P<.001), height and weight: FAS < HE and controls (P < .03), BMI FAS < HE and controls (P < .01), palpebral fissure length FAS < HE and controls (P < .0001), flat philtrum and thin vermillion FAS < HE and controls (p<0.05) and FSIQ FAS and HE < controls (p<.0006). Diagnostic severity relations for brain measures: left and right caudate volume FAS and HE < controls (p<.001), total intracranial volume FAS < control (p<.002) and HE < control (p = 0.03). There were no significant left-right caudate volume differences for any of the groups either controlled by gender or mixed.

	FAS (n=22)	HE (n=50)	Control (n=47)	F
Age at 3D photo (years)	13.0 ± 3.2	12.3 ± 2.2	12.6 ± 2.3	0.84
Age at MRI image (years)	12.6 ± 3.2	12.2 ± 2.0	12.6 ± 2.3	1.26
3D-MRI difference (months)	2.0 ± 2.1	3.2 ± 4.6	4.2 ± 4.7	1.90
Sex n (% male)	10 (45.5%)	36 (72.0%)	26 (45.5%)	2.17
Height (cm)	136.7 ± 18	147.1 ± 18	154.1 ± 14.8	8.18***
Wt (kg)	33.7 ± 11.6	45 ± 19	50.0 ± 15.0	7.47***
Head circumference (cm)	51 ± 1.8	53.6 ± 2.5	54.9 ± 2.0	22.49***
BMI	17.3 ± 2.2	19.9 ± 4.4	20.6 ± 4.0	5.34**
Facial anomalies				
Palpebral **fissure length**	19 (86.4%)	8 (16%)	4 (8.5%)	39.73***
Smooth philtrum	12 (54.5%)	11 (22%)	9 (19.1%)	6.19**
Thin vermillion	12 (54.5%)	14 (28%)	11 (23.4%)	3.13*
Brain measures				
Left caudate volume (mm3)	3307 ± 669	3714 ± 566	4048 ± 471	13.27***
Right caudate volume (mm3)	3361 ± 693	3800 ± 577	4713 ± 499	10.59***
Corpus Callosum volume (mm3)	15994 ± 3622	18838 ± 3035	21131 ± 3794	14.21***
Total cranial volume (mm3)	1173365 ± 230611	1267130 ± 280067	1373410 ± 235361	4.09*
General Cognitive Ability (Std score)	90.5 ± 45.1	90.9 ± 45.9	109.8 ± 56.2	3.133***

* P < 0.05.

** P < 0.01.

*** P < 0.001.

Table 3.

Separate face and brain control-FAS discrimination rates estimated as the mean area under the ROC curves of 20 cross-validation tests, corresponding to the probability of accurately classifying pairs of individuals: 1 from control and 1 from FAS. Full face and facial regions achieved high discrimination rates as did corpus callosum and caudate nucleus.

FACE	CM	LDA	SVM		BRAIN	CM	LDA	SVM
Full Face	0.93	0.93	0.95		Corpus Callosum	0.90	0.90	0.93
Profile	0.83	0.88	0.90		Caudate Nucleus	0.88	0.88	0.88
Eyes	0.90	0.93	0.93		Left Caudate Nucleus	0.83	0.85	0.90
Malar	0.95	0.95	0.93		Right Caudate Nucleus	0.83	0.85	0.90
Mandible	0.88	0.88	0.90					
Nose	0.95	0.95	0.98					
Lip Vermilion	0.85	0.85	0.85					
Philtrum	0.83	0.83	0.88					

Table 4.

Combined face-brain discrimination rates (mean area under the ROC curves of 20 cross-validation tests) correspond to the probability of correctly classifying pairs of individuals - 1 control and 1 from the FAS set. Testing for the full face and localised facial regions combined with corpus callosum, whole caudate nucleus and left caudate nucleus revealed high discrimination rates and improved accuracy compared to analogous testing on face and brain components separately.

	+CC			+CN			+LEFT CN			+RIGHT CN		
	CM	**LDA**	**SVM**	**CM**	**LDA**	**SVM**	**CM**	**LDA**	**SVM**	**CM**	**LDA**	**SVM**
Full Face	0.90	0.90	0.93	0.90	0.90	0.90	0.95	0.95	0.95	0.90	0.90	0.93
Profile	0.90	0.90	0.88	0.85	0.85	0.88	0.95	0.95	0.95	0.90	0.90	0.90
Eyes	0.90	0.93	0.93	0.90	0.90	0.90	0.95	0.95	0.98	0.95	0.95	0.95
Malar	0.90	0.93	0.93	0.90	0.90	0.93	0.98	0.95	0.95	0.93	0.93	0.93
Mandible	0.88	0.88	0.90	0.88	0.88	0.88	0.95	0.95	0.95	0.90	0.90	0.93
Nose	1.00	1.00	1.00	0.93	0.93	0.88	0.95	0.95	0.95	0.93	0.93	0.93
Lip Vermilion	0.90	0.90	0.90	0.85	0.85	0.93	0.95	0.95	0.95	0.85	0.85	0.88
Philtrum	0.95	0.98	0.98	0.85	0.85	0.88	0.95	0.95	0.95	0.90	0.90	0.88